Urban–rural gradients reveal joint control of elevated CO₂ and temperature on extended photosynthetic seasons

Songhan Wang [1,2,3], Weimin Ju[1,2], Josep Peñuelas [4,5], Alessandro Cescatti[6], Yuyu Zhou[7], Yongshuo Fu [8], Alfredo Huete[9], Min Liu[10,11] and Yongguang Zhang [1,2,3]*
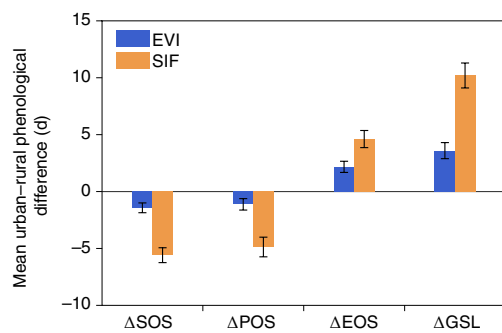
Photosynthetic phenology has large effects on the land–atmosphere carbon exchange. Due to limited experimental assessments, a comprehensive understanding of the variations of photosynthetic phenology under future climate and its associated controlling factors is still missing, despite its high sensitivities to climate. Here, we develop an approach that uses cities as natural laboratories, since plants in urban areas are often exposed to higher temperatures and carbon dioxide (CO_2) concentrations, which reflect expected future environmental conditions. Using more than 880 urban–rural gradients across the Northern Hemisphere ($\geq 30°$N), combined with concurrent satellite retrievals of Sun-induced chlorophyll fluorescence (SIF) and atmospheric CO_2, we investigated the combined impacts of elevated CO_2 and temperature on photosynthetic phenology at the large scale. The results showed that, under urban conditions of elevated CO_2 and temperature, vegetation photosynthetic activity began earlier (-5.6 ± 0.7 d), peaked earlier (-4.9 ± 0.9 d) and ended later (4.6 ± 0.8 d) than in neighbouring rural areas, with a striking two- to fourfold higher climate sensitivity than greenness phenology. The earlier start and peak of season were sensitive to both the enhancements of CO_2 and temperature, whereas the delayed end of season was mainly attributed to CO_2 enrichments. We used these sensitivities to project phenology shifts under four Representative Concentration Pathway climate scenarios, predicting that vegetation will have prolonged photosynthetic seasons in the coming two decades. This observation-driven study indicates that realistic urban environments, together with SIF observations, provide a promising method for studying vegetation physiology under future climate change.

Terrestrial ecosystems absorb approximately one-quarter of the anthropogenic carbon dioxide (CO_2) released into the atmosphere, which effectively mitigates climate warming[1]. The timing and duration of vegetation photosynthetic activity (that is, photosynthetic phenology) play an important role in the carbon cycle of land ecosystems[2,3] and are strongly affected by climate change[4–7]. Therefore, understanding the response of photosynthetic phenology to increasing atmospheric CO_2 concentrations and global warming is essential, to better understand the future dynamics of the terrestrial carbon cycle[8,9] and formulate land-based strategies to mitigate climate change[10]. Current experimental assessments of the effects of climate warming and CO_2 fertilization on plant phenology have generally been restricted to manipulated experiments[11,12] with very limited spatial extent and species coverage, which may ultimately lead to ambiguous and controversial findings[13]. In particular, the role of CO_2 fertilization on tree phenology remains largely unknown in real, natural settings. Moreover, many field experiments have recently been terminated because of their high cost[14], thus limiting consistent long-term observations and reinforcing the need for effective, low-cost alternative monitoring approaches.

In this analysis, we make use of contrasting conditions in urban–rural environments, serving as 'natural laboratories' for conducting

a novel investigation of the combined effects of future global warming and CO_2 fertilization on vegetation phenology at a very large scale[14]. Because of the urban heat island effect[15] and the larger CO_2 emissions from fossil fuel combustion[16], vegetation in urban areas is typically exposed to higher temperatures and CO_2 concentrations than in rural areas. Urban areas are therefore experiencing growing conditions projected for the future[17]. Assuming that phenology responds similarly to altered temperature and atmospheric CO_2 in urban and rural areas, the urban–rural gradients can be considered as 'natural experiments' with similar photoperiods and weather, and at lower costs[14] than manipulation experiments. Using the space-for-time substitution concept, we therefore used the physiological dynamics of vegetation across urban–rural gradients to investigate the effects of future global warming and CO_2 fertilization on photosynthetic phenology. Data were collected from 880 urban clusters and their adjacent rural areas at mid- to high latitudes in the Northern Hemisphere ($\geq 30°$N) (Supplementary Fig. 1). Photosynthetic phenology was extracted from the Orbiting Carbon Observatory-2 (OCO-2)[18] Sun-induced chlorophyll fluorescence (SIF; a proxy for photosynthesis) data, which are highly correlated with photosynthetic rates and can monitor actual photosynthetic dynamics[19]. We used the traditional, satellite greenness phenology

Fig. 1 | Mean urban–rural phenological differences based on SIF and EVI. Differences in phenological indicators between urban areas and rural buffers are indicated by '∆' (for example, $\Delta SOS = SOS_{urban} - SOS_{rural}$). Error bars represent s.e.m. ($n = 880$).

data for comparison, which were extracted from the Moderate Resolution Imaging Spectroradiometer (MODIS) enhanced vegetation index (EVI)[20]. The urban–rural surface CO_2 gradients were obtained through a conversion approach with OCO-2 column-averaged CO_2 mixing ratios (XCO$_2$) data (see Methods). The primary objectives of our analysis were to determine the differences in photosynthetic phenology across urban–rural gradients and to explore the combined effect of atmospheric CO_2 enrichment and warming on plant photosynthetic phenology at a very large scale. Phenological differences and environmental gradients were then used to quantify the sensitivities of the processes, and ultimately to project shifts in phenophases under contrasting climate scenarios.

Results

We found that vegetation showed a larger than expected anticipation and prolongation of the photosynthetic season within urban environments. On average, the SIF-based photosynthetic activity began 5.6 d earlier, peaked 4.9 d earlier, ended 4.6 d later and lasted 10.2 d longer in urban compared with rural areas (Fig. 1). These variations were two to four times larger than those in greenness phenology derived from MODIS EVI, due to the significantly higher urban–rural ∆SIF than ∆EVI during spring and autumn (Supplementary Fig. 2). The timings of each phenological indicator we examined (start of growing season (SOS), peak of growing season (POS), end of growing season (EOS) and length of growing season (GSL)) were generally highly correlated between urban areas and neighbouring rural counterparts, but with significant systematic deviations, as indicated by the slopes of the regression lines (Supplementary Fig. 3). The SOS and POS occurred earlier in urban areas, as suggested by the slopes of >1 (that is, 1.01–1.03 and 1.00–1.02; $P < 0.001$) for the regression lines, whereas the EOS occurred later in urban areas, as indicated by the slopes of <1 (that is, 0.98–0.99; $P < 0.001$). On average within cities, SOS and POS were therefore advanced, while EOS was delayed and GSL was extended for the phenology of SIF. Similar patterns were found for the phenology of EVI, but the magnitudes of these changes were substantially smaller than that of SIF (Supplementary Fig. 4) (about fourfold for ∆SOS and ∆POS, twofold for ∆EOS and threefold for ∆GSL; Fig. 1). The larger differences of photosynthetic phenology in urban–rural gradients than the differences of greenness phenology were not affected by the mismatching in the spatial resolutions of the SIF and EVI data, as also tested after resampling to the same resolution (Supplementary Fig. 5). These results suggest a remarkable shift in the response of photosynthetic phenology to urban environmental conditions in the mid- to high latitudes of the Northern Hemisphere. These variations cannot be completely explained by the variations in greenness

phenology based on vegetation indices or leaf area index, and probably involve physiological responses to environmental drivers.

Vegetation in urban areas generally had earlier photosynthetic SOS and POS, later EOS and longer GSL in the Northern Hemisphere across various latitudes and climatic backgrounds (Fig. 2). On average, more than 70% of the urban clusters had longer photosynthetic seasons than rural buffers. ∆SOS and ∆POS were lower than zero days across the whole Northern Hemisphere, while most of the ∆EOS values were greater than zero days, suggesting that the trends of an earlier start and peak of photosynthesis and delayed end of photosynthesis in urban environments are common across northern latitudes. Nevertheless, some spatial patterns of phenological shifts along urban–rural gradients were also evident. ∆SOS tended to decrease slightly as latitude increased. ∆EOS and ∆GSL had the highest values at mid-latitudes, whereas ∆POS had no clear trend (second column in Fig. 2). The spatial patterns of SIF ∆SOS were not fully consistent with previous studies conducted with EVI, which showed an increasing trend of EVI ∆SOS with latitude[21] due to the larger urban heat island effects in high latitudes[15,22]. This divergence possibly suggests that the spatial distributions of SIF urban–rural phenological gradients cannot be explained by temperature alone. Importantly, urban–rural phenological differences were more significant in warm and dry regions (that is, areas with high mean annual air temperature and low annual precipitation) than in other regions (third column in Fig. 2). Thus, the phenological differences in arid climate zones were significantly higher than in temperate and boreal areas (Supplementary Fig. 6). These results suggest a general phenomenon that urban environmental conditions extend the photosynthetic seasons and that the impacts in warm and dry regions are greater than those in other climate regions.

Urban–rural phenological differences are probably driven by several interacting factors, including enhancements of temperature and CO_2, the geolocation of a city, urban size and climatic background. Partial correlation analysis showed that SIF ∆SOS and ∆POS were mainly controlled by the daytime urban heat island effects (ΔLST_{day}, where LST is the land surface temperature) and urban–rural CO_2 gradients (ΔCO_2), of which ΔLST_{day} was the most significant (Fig. 3). SIF ∆EOS was mainly attributed to the enhanced CO_2 only, resulting in similarly significant effects of temperature and CO_2 on ∆GSL (Fig. 3). To attribute the effects of environmental drivers on photosynthetic phenology, we further analysed the associations between elevated daytime temperature or atmospheric CO_2 and urban–rural phenological differences (Fig. 4). The onset and peak time of photosynthesis were both advanced significantly as atmospheric CO_2 concentration increased ($P = 0.013$ and $P = 0.021$, respectively) and as temperature increased ($P = 0.019$ and $P = 0.006$, respectively). The end of photosynthetic activity was significantly delayed as CO_2 concentrations increased ($P = 0.028$), whereas its association with temperature was not significant ($P = 0.259$). Our analyses suggest that not only daytime temperature but also atmospheric CO_2 have large impacts on photosynthetic phenology of urban plants and, therefore, may potentially inform about the future phenological shifts of natural vegetation under scenarios of warming and atmospheric CO_2 enrichment.

Finally, using observations along the urban–rural gradients as natural laboratories, we projected the shifts in photosynthetic phenology for the next two decades using the space-for-time substitution. Based on forward stepwise regression models (see Methods), the sensitivities of ∆SOS, ∆POS and ∆GSL to daytime temperature were -1.55 ± 0.60, -2.11 ± 0.78 and $3.31 \pm 1.10\,d\,°C^{-1}$, respectively (Fig. 5a). The sensitivities of ∆SOS, ∆POS, ∆EOS and ∆GSL to surface CO_2 concentration were -0.15 ± 0.07, -0.18 ± 0.09, 0.17 ± 0.07 and $0.32 \pm 0.11\,d\,ppm^{-1}$, respectively (Fig. 5b). Given the observed sensitivities and four different Representative Concentration Pathway (RCP) scenarios of surface temperature and CO_2 concentration[10]
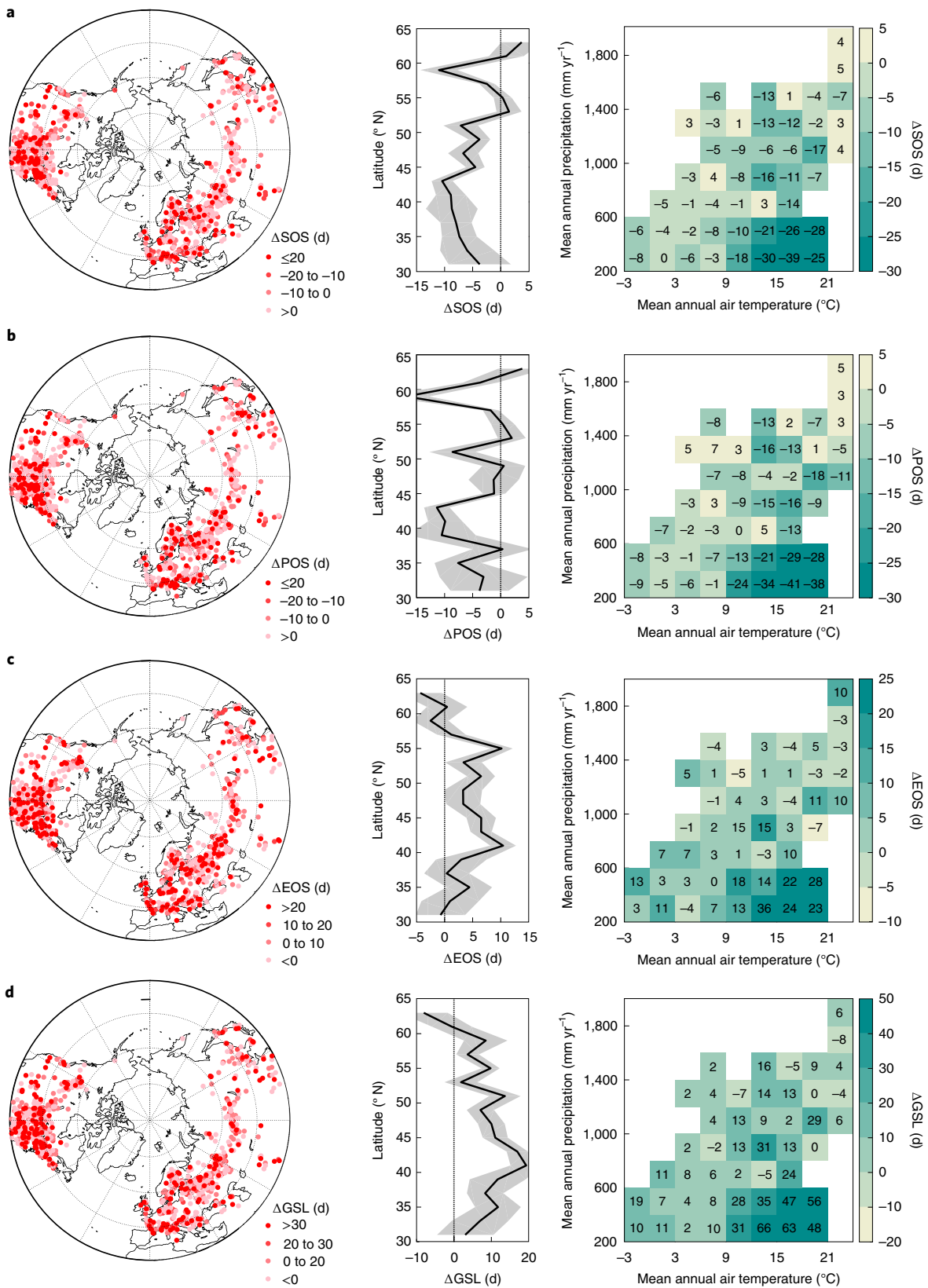
Fig. 2 | Spatial distributions of the four urban–rural phenological differences based on SIF. a–d, Spatial distributions of ΔSOS (**a**), ΔPOS (**b**), ΔEOS (**c**) and ΔGSL (**d**) for SIF (*n* = 880). Left, urban effects on phenological metrics for various urban clusters. Middle, phenological differences based on latitudinal profiles (shaded areas represent s.e.m.). Right, average metrics for two varying climatic backgrounds (mean annual air temperature and precipitation).
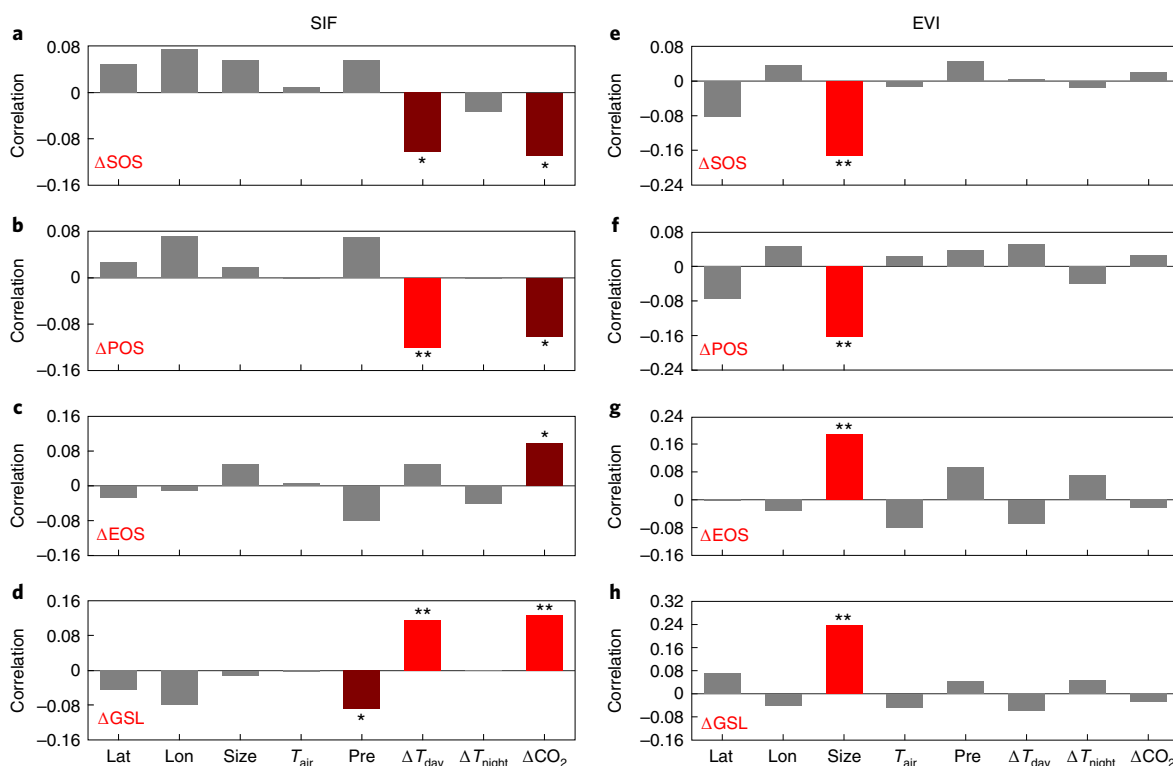
Fig. 3 | Controlling factors of urban–rural phenological differences. a–h, Partial correlations of SIF (**a–d**) and EVI (**b–h**) urban–rural phenological differences (ΔSOS (**a** and **e**), ΔPOS (**b** and **f**), ΔEOS (**c** and **g**) and ΔGSL (**d** and **h**)) with explanatory variables. ΔCO_2, urban–rural CO_2 difference; lat, latitude; lon, longitude; pre, mean annual precipitation; size, $\log_{10}$ of the urban size; T_{air}, mean annual air temperature; ΔT_{day}, daytime urban–rural LST difference; ΔT_{night}, night-time urban–rural LST difference. *$P < 0.05$; **$P < 0.01$ ($n = 880$).

(that is, RCPs 2.6, 4.5, 6.0 and 8.5; Supplementary Fig. 7), we projected the possible shifts of photosynthetic SOS, POS, EOS and GSL from 2015–2035 (Fig. 5c–f). The results show that the phenophase shifts were lowest under the RCP 2.6 scenario and highest under the RCP 8.5 scenario. Assuming constant sensitivities for the next two decades, under the range of climate pathways foreseen by RCP scenarios during 2015–2035, the photosynthetic SOS and POS would advance at a rate of 2.8–5.7 and 3.3–6.9 d decade^{-1}, respectively, and the EOS would delay at a rate of 3.1–5.7 d decade^{-1}, prolonging the growing season by a rate of 5.9–11.4 d decade^{-1} (Fig. 5g). It should be noted that the responses of vegetation phenology to temperature are not stationary[23] and are likely to decline in the near decades[9,24]. Besides this, the sensitivity of vegetation phenology to CO_2 may not be static either in the coming decades, since the projected future concentrations of CO_2 could exceed the range currently experienced by urban vegetation (Fig. 4 and Supplementary Fig. 7b). Therefore, our analysis of the projected photosynthetic phenology based on the static sensitivity may overestimate the future shifts of vegetation phenophases. However, this caveat can be solved in the future using the same procedure introduced in this study and continued satellite SIF observations.

Discussion

We found systematic differences between urban–rural gradients of photosynthetic and greenness phenology (Fig. 1). The urbanization effects on vegetation photosynthetic phenology were more than twofold higher than those on greenness. This phenomenon could be explained by the significant differences between season cycles of EVI and SIF; namely, EVI shows an earlier spring increase and a later autumn falling than SIF (Supplementary Fig. 2a). This difference has also been demonstrated by a recent study[25]. The timing of carbon assimilation in spring lags behind the leaf burst, which

varies with foliar structure and longevity[26]. The photosynthetic activity shuts down before the reduction of leaf chlorophyll and leaf abscission because of the limitation of light availability[27–29]. Another possible reason is that urban phenology indicators from vegetation indices are suffering from mixed-pixel effects[30], which can bias the gradients of urban–rural greenness phenology. Besides, vegetation indices may have noisy signals from soil background, such as soil colour, artificial green building and other non-photosynthetic active materials, especially in urban areas[31–33]. In contrast, originating from the vegetation photosynthetic pigments, SIF is less sensitive to the soil background[34–36].

Our analyses suggest that the urban–rural photosynthetic phenological differences are mainly controlled by elevated atmospheric CO_2 concentration and daytime temperature, while the differences of greenness phenology mostly depend on urban size (Fig. 3). Previous studies using dozens of cities at the regional scale suggest a positive correlation between earlier greenup and surface temperature enhancement of urban areas, such as in eastern North America[37,38] and China[21,39,40]. However, our analysis shows that the urban–rural greenness phenological differences are mainly correlated with urban size in the Northern Hemisphere, which is in line with a recent study conducted with thousands of cities in the conterminous United States[41]. The positive relationship between urban–rural greenness phenological gradients and urban size (an indicator of urbanization) may result from the shifts of vegetation percentages and regional climate conditions induced by urban expansion[41]. In contrast, the earlier start and peak of photosynthesis activity inferred from SIF observations are significantly correlated with elevated temperature in urban areas (Fig. 4a,b). This discrepancy might partly relate to the different sensitivity of vegetation indices and SIF to temperature increases, either based on satellite data[25] or previous site-level studies[42]. More importantly, SIF has a positive
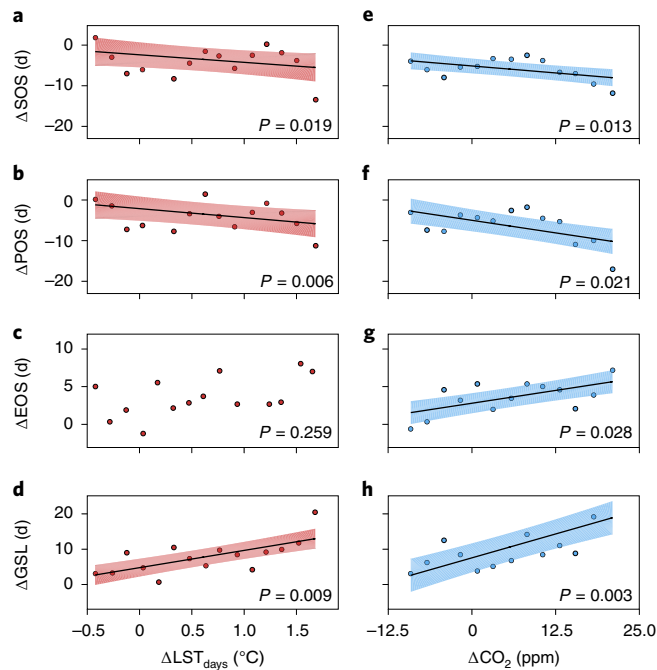
Fig. 4 | Temperature and CO$_2$ associations with the phenological gradients. a–h, Associations between elevated temperature (**a–d**) and CO$_2$ (**e–h**) and the urban–rural photosynthetic phenological gradients (ΔSOS (**a** and **e**), ΔPOS (**b** and **f**), ΔEOS (**c** and **g**) and ΔGSL (**d** and **h**)). The LST and CO$_2$ gradients are binned every 0.15 °C and 1.5 ppm, respectively, and each dot represents a bin. The solid lines indicate significant trends and the shaded areas represent 95% confidence intervals. Significance was determined by Student's t-test ($n = 880$).

Fig. 5 | Future projections of photosynthetic phenology shifts. a,b, Projected shifts in photosynthetic phenology during the next two decades. Sensitivities of photosynthetic phenology to temperature (**a**) and CO$_2$ (**b**) are shown. Error bars represent s.e.m. **c–f,** Shifts of photosynthetic SOS (**c**), POS (**d**), EOS (**e**) and GSL (**f**) from 2015–2035, as calculated from the sensitivities shown in **a** and **b**, as well as and LST and CO$_2$ concentration predictions during 2015–2035 from four RCP scenarios. Shaded areas represent s.e.m. **g,** Projected shifts of photosynthetic phenology during the next two decades. Negative values represent advances of SOS and POS, and positive values represent delayed EOS and prolonged GSL. Error bars represent s.e.m.

correlation with gross primary productivity (GPP), both at the leaf and site level[19,43,44], which is a more direct indicator of vegetation physiological status than are vegetation indices[45]. The seasonality of SIF from ground-based measurements[46], tower-based observations[47] and satellite-based data[25] is generally highly correlated with the seasonality of GPP. Therefore, SIF-based photosynthetic phenology in studies of 'urban laboratories' could provide a better proxy of the actual vegetation photosynthetic changes in response to climate change than vegetation indices, which provide proxies of vegetation greenness.

Using 880 cities, our results confirm that vegetation photosynthesis activities in spring are triggered by daytime temperature, not by night-time temperature[8] (Fig. 3). However, the sensitivity of SOS to daytime temperature in this study (1.55 ± 0.60 d °C^{-1}) is lower than in previous studies for boreal and temperate forests, based on long-term satellite vegetation indices or ground observations[8,9,48–52]. This may reflect the declining warming effects on spring leaf unfolding[9] and weakening temperature control on the interannual variations of vegetation spring carbon uptake[53]. The reduced sensitivity of spring leaf unfolding to temperature may partly result from the reduced chilling accumulation in urban areas[9], in which the winter temperatures may become insufficiently low to meet the requirement of chilling due to the urban heat island effects. Photoperiod may also influence the warming effects on spring phenology, although its impact remains unclear and is under debate[5,23,54,55]. We also found that photosynthetic POS has an earlier trend (about 3.3–6.9 d decade^{-1}) in the near decades, which is consistent with the POS trend of δ^{13}C data (about 4.3 ± 2.9 d decade^{-1})[56] and larger than the POS trends from normalized difference vegetation index data or ground phenology measurements[48,56,57].

This phenomenon highlights the advantages of SIF for tracking vegetation seasonal photosynthetic activities and carbon uptake. Our analysis also reveals a delayed end of vegetation photosynthesis in urban areas (Fig. 1). Other than the earlier start of SOS and its response to global warming, our understanding of the drivers for delayed EOS is still limited. Temperature[12,58], photoperiod[59], elevated atmospheric CO$_2$[60] and spring phenology[61] have all been associated with this delayed vegetation senescence. Nevertheless, our analysis suggests a pronounced delay in the end of vegetation photosynthesis in urban environments, and these delays are highly correlated with the elevated atmospheric CO$_2$ concentration.

Current studies generally focus on the responses of phenophases to warming[9,13], ignoring the importance of additional environmental drivers. From this point of view, our analysis highlights that photosynthetic phenological shifts are not only controlled by daytime

temperature, but also by atmospheric CO_2. CO_2 fertilization seems to have a large effect on the advancement of photosynthetic activity, particularly under warm and dry conditions, and the delayed end of photosynthesis is mainly attributed to the elevated atmospheric CO_2 rather than temperature, which is consistent with field experiments[62–64]. The delayed EOS may be because photosynthesis could be sustained for longer periods in the absence of sink limitations under elevated atmospheric CO_2 concentrations[64]. However, direct evaluations of the future projected phenophase shifts are difficult, given global increases in the CO_2 concentration and temperature of 16.5 ppm decade^{-1} and 0.16 °C decade^{-1}, respectively, over the past three decades[65] (1982–2011). Our estimate of the prolonged photosynthetic growing season (5.5 ± 2.1 d decade^{-1}) is significantly higher than current estimates (2.2–3.9 d decade^{-1}) based on long-term satellite vegetation indices[66,67], as well as the in situ experimental results based on greenness observations from a recent study[5]. Our results suggest that the sensitivity of photosynthetic phenology to climate is strikingly higher than that of traditional greenness phenology, and therefore, that the current methods based on satellite vegetation indices and in situ greenness observations are likely to underestimate the extension of the carbon sink period under climate change. Crucially, our results show that, with increasing atmospheric CO_2, the growing seasons are likely to expand in the next two decades, which in turn might contribute to an increasing trend of the terrestrial carbon sink, as well as generating an important negative feedback in the climate system.

It should be noted that some limitations still remain in our analysis. Landscape configuration, species composition[68], atmospheric deposition (for example, nitrogen and phosphorus), air pollutants (for example, ozone), management practices and hydrological regimes may also affect urban–rural phenological differences. These factors may have complex and, to some extent, counterbalanced impacts on vegetation photosynthesis in urban environments. For example, urban areas generally receive higher rates of atmospheric nitrogen and phosphorus deposition[69], which may positively contribute to urban–rural phenological differences (Supplementary Fig. 8b). In contrast, urban areas typically show higher daytime ozone concentrations that can be detrimental to photosynthesis[70], and these urban–rural ozone differences may negatively contribute to the urban–rural phenological differences (Supplementary Fig. 8c). Additionally, vegetation species and human management practices may vary between urban and rural areas and, apart from the temperature and CO_2, water stress indices such as precipitation, vapour pressure deficit and soil moisture may also influence vegetation phenology[71–73]. Urban–rural phenological gradients in areas with low precipitation are generally more pronounced (Supplementary Fig. 8a) because vegetation in urban areas is likely to be affected by irrigation and thus not limited by water supply. To test whether our results were affected by the irrigation of urban vegetation, we repeated the analysis after excluding the cities in the arid climate zones, assuming that the irrigation effect on urban–rural phenology gradients could be more significant in these areas. These results also showed that the extended photosynthetic seasons in urban areas were controlled by both the elevated temperature and CO_2 (Supplementary Fig. 9a), but with slightly lower sensitivities. Therefore, our predictions of the GSL shifts based on all of the 880 cities may be slightly overestimated at a rate of about 0.8–1.2 d decade^{-1} (Supplementary Fig. 9b). Moreover, to verify the robustness of our analysis, we further calculated the phenological differences between the 10 and 30-km rural buffers, and related them to temperature and CO_2 gradients. The results showed higher correlations with temperature and CO_2 compared with the original urban–rural gradients (Supplementary Fig. 10). These higher correlations not only confirm the robustness of our analysis, but also suggest that the confounding factors (for example, vegetation species, irrigation and nutrient supply) do not affect the controlling role of temperature and CO_2 in vegetation photosynthetic phenology, given that the vegetation phenology in 10-km rural buffers is less influenced by these factors than in urban areas. However, these confounding factors can hardly be included in our analysis due to the lack of high-resolution data at the global scale.

The novel insights of this study were derived at a large scale from the contrasting behaviour of plants along urban–rural gradients. The sharp differences in environmental conditions along these gradients can represent a unique 'natural laboratory' with different atmospheric CO_2 concentrations and temperatures that may ultimately inform on plant behaviours under future climates and atmospheric compositions. The macro-environmental conditions of open urban laboratories are widely reachable around the globe and can therefore lead to more general and robust assessments of vegetation responses to key environmental drivers across different environmental conditions from a global-change perspective. Ultimately, our findings shed new light on the behaviour of plants under global change, help to reduce the uncertainties of terrestrial ecosystems models[74], and increase our understanding of climate–vegetation interactions.

Methods

Urban–rural gradients. We focused our study on urban clusters and their adjacent rural buffers at mid- to high latitudes in the Northern Hemisphere (≥30° N) from 2015–2017 (Supplementary Fig. 1), where vegetation is highly seasonal and sensitive to climate[61,66]. The extents of the urban areas were mapped using a cluster-based method that estimates optimum thresholds using night-time stable-light data from the Defense Meteorological Satellite Program/Operational Linescan System[75]. Sensitivity analyses and comparisons with other global urban-area products indicated that this product is reliable and highly accurate[76]. We used this data product (for 2013) instead of extracting urban areas from land cover datasets, because these cluster-based urban extents clearly define the boundaries between urban and rural areas, regardless of the internal spatial heterogeneity, which is more similar to the real environment than the vegetation experiences. Although the static urban clusters (2013) and our study period (2015–2017) differed by approximately three years, the overall results should not be affected due to almost stable urban clusters in North America and Europe[41] and the slightly increasing urban areas in Asia[77].

We created a series of buffers extending 10, 20, 30 and 40 km outward from each urban cluster perimeter to select an appropriate threshold for SIF data. Because of the limited spatial coverage of the OCO-2 SIF data, we used an interval of 10 km to ensure that each buffer had a sufficient number of observations. An example of the urban cluster and its corresponding rural buffers is shown in Supplementary Fig. 11. Pixels representing water body or crops were excluded from this analysis (Supplementary Fig. 11a). Croplands were excluded because their photosynthetic dynamics are strongly affected by human management. We also excluded pixels in rural areas that had elevations 50 m greater or less than the average elevation of urban pixels (for both SIF and EVI data; Supplementary Fig. 11b)[21]. Given that the number of OCO-2 SIF observations per year was low, we opted for the use of SIF data in each urban cluster and its corresponding rural buffers from 2015–2017 as one completed phenological cycle. OCO-2 footprints with viewing zenith angles of <20° in glint and target modes were used[78]. We selected urban clusters with at least eight SIF observations in both the urban cluster and each corresponding buffer to ensure a successful calculation of phenology. This resulted in a total of 880 urban clusters (Supplementary Fig. 1).

Data. We used the OCO-2 SIF Lite product (B8100) at 757 nm for 2015–2017. OCO-2 is a Sun-synchronous polar-orbit satellite launched in July 2014, with an altitude of 705 km and a descending node at approximately 13:30 local time[18]. OCO-2 leads the 'A-Train' satellite constellation with a repeating cycle of approximately 16 d. The instrument collects high-resolution radiance spectra in the O_2-A band (757–775 nm), which can be used to retrieve fluorescence signals from vegetation. Retrievals based on the in-filling of solar Fraunhofer lines in narrow spectral windows around 757 and 771 nm were conducted using the singular vector decomposition method. The accuracy of single measurements at 757 nm after a series of bias-correction and quality-control steps is approximately 15–25% of the typical peak values of SIF[18]. However, because there are dozens of single measurements in each urban cluster and the corresponding rural buffer, most of the noise in the retrieved SIF was reduced following the $1/\sqrt{n}$ law, which means that the precision errors in the average of n samples will be reduced by a factor of $1/\sqrt{n}$[79]. Moreover, the relative uncertainties of single measurement in the urban clusters and rural buffers are almost identical (Supplementary Fig. 12); therefore, the retrieval errors of SIF should not have large impacts on the urban–rural phenological patterns. We chose the SIF data at 757 nm because the signals are approximately 1.5-fold greater at 757 nm than those at 771 nm.

The data for Aqua MODIS EVI collection 6 (MYD13A2; 16-d composite) with a spatial resolution of 1 km for 2015–2017 were used to extract greenness phenology information. The EVI data partially eliminate the effects of canopy background, and remain sensitive to small changes in vegetation activity compared with normalized difference vegetation index data[20]. Thus, the EVI data are considered to be more appropriate for use in areas with sparse vegetation coverage, such as urban clusters[21,38]. We used the Aqua EVI data to maintain consistency with the OCO-2 overpass time (both occur at approximately 13:30 local time). To make a comparison, the MODIS EVI data were selected according to the same OCO-2 overpasses. To test whether the observed urban–rural phenological patterns were an artefact of the difference in spatial resolutions between OCO-2 SIF and MODIS EVI, we resampled both SIF and EVI data to a spatial resolution of 5 km and reproduced the urban–rural phenological differences. The results also showed larger differences of photosynthetic phenology in urban–rural gradients than the differences of greenness phenology (Supplementary Fig. 5), and thus provide support for the robustness of our analysis.

We obtained the urban–rural XCO_2 gradients using reprocessed Lite files from the OCO-2 product (version 8r) for 2015–2017. The data were bias-corrected using observations from the Total Carbon Column Observing Network. OCO-2 also collects high-resolution radiance spectra at the 1.61- and 2.06-µm bands, except for the O_2-A band, which can be used to retrieve XCO_2[80] based on the Atmospheric CO_2 Observations from Space algorithm. Comparisons with the measurements at Total Carbon Column Observing Network sites showed that the precision of the Lite products was approximately 1.5 ppm[81].

We used the Aqua MODIS collection 6 LST dataset (MYD11A2; 8-d composite) with a spatial resolution of 1 km for 2015–2017 to calculate the urban–rural LST gradient. We chose LST data from the Aqua satellite because its data were acquired at 13:30 and 01:30 local time each day, approximately representing the diurnal and nocturnal temperatures, respectively (that is, maximum and minimum temperatures). We also used the air surface temperature (AST) data from the TerraClimate dataset[82] with a spatial resolution of 4 km to calculate the urban–rural AST gradient.

We also extracted the mean annual air temperature (2 m above the surface) for each urban cluster from the analytical dataset based on both the Global Historical Climatology Network (version 2) and the Climate Anomaly Monitoring System, with a spatial resolution of 0.5°. The annual precipitation of each urban area was calculated based on the monthly Integrated Multi-satellite Retrievals dataset from global precipitation measurements, with a spatial resolution of 0.1°. Digital elevation models at a spatial resolution of 30 arcsec from the GTOPO30 dataset and the land cover dataset for 2015 from the European Space Agency Climate Change Initiative were also used in this study. We also used the global gridded nitrogen dioxide (NO_2) and ozone (O_3) observations from the Ozone Monitoring Instrument. We calculated the mean LST changes for 2015–2035 at mid- to high latitudes in the Northern Hemisphere ($\geq 30°$ N) from four Earth system models (CSIRO-Mk3.6.0 (ref. [83]), GFDL-CM3 (ref. [84]), GISS-E2-H[85] and NorESM1-M[86]) within Coupled Model Intercomparison Project Phase 5. Projected CO_2 concentration changes from 2015 were obtained from the RCP Database. Detailed information on the datasets is presented in Supplementary Table 1.

Extraction of phenological data. We used a double-sigmoidal function to fit the annual cycles of the SIF and EVI observations[87]. Choosing an appropriate method to fit noisy SIF data is important because of the wide variation in phenology when estimated with different methods. We chose the double-sigmoidal method for three reasons. First, the speeds of spring leaf out and autumn senescence are not always the same: leaf out is generally faster than senescence[88]. The double-sigmoidal method can identify the actual biophysical dynamics of vegetation by setting two amplitudes for spring and autumn[87]. Second, functional fitting methods have advantages for estimating phenology with noisy data[89]. The OCO-2 data are acquired at different time intervals and are relatively noisy, and the number of observations is small. Thus, some fitting approaches, such as polynomial fitting, logistic fitting and harmonic analysis, cannot be used or cannot converge to the global optimum. Third, the double-sigmoidal method has been successfully applied to SIF data in a previous study[33]. The fitting equation is[56,87]:

$$y(t) = a_1 + \frac{a_2}{1 + \exp(-d_1(t - b_1))} - \frac{a_3}{1 + \exp(-d_2(t - b_2))} \quad (1)$$

where $y(t)$ represents the observed SIF or EVI for a given day of year (t), a_1 represents the value in the winter dormant period, a_2 represents the value at the spring and early summer plateau, a_3 represents the value at the late summer and autumn plateau, b_1 and b_2 are the day of the year mid-points of transitions for spring leaf out and autumn senescence, respectively, and d_1 and d_2 are the corresponding slope coefficients of these transitions.

The fitting equation was adapted to our SIF and EVI time series, and the coefficients were optimized using genetic algorithms. A simple weighting scheme was applied to the noisy data. We assigned a weight of two if a central point was within $\pm 50\%$ of the median for a moving window of three points[33]. A maximum of 20 fitting attempts with different initial values were made until the fitting procedure converged to the global optimum. Each attempt had a maximum of

2,000 iterations. The R^2 values of SIF fitting were lower than those of EVI, but most were larger than 0.8 (Supplementary Fig. 13). The R^2 values were generally high for the EVI data. The phenological indicators were then determined using[56]:

$$SOS = b_1 - \frac{4.562}{2d_1}$$

$$POS = 1.317\left(-\left|\frac{1}{a_1}\right| + b_1\right) \quad (2)$$

$$EOS = b_2 + \frac{4.562}{2d_2}$$

$$GSL = EOS - SOS$$

An example of the fitting method and the estimation of phenological indicators is shown in Supplementary Fig. 14a. We excluded some extreme values using a loose threshold to reduce uncertainties, and slightly adjusted the thresholds based on previous studies[21,38,41] due to the differences between the data and methods. SOSs earlier than the 30th or later than the 180th day of the year, and EOSs earlier than the 240th or later than the 350th day of the year, were thus excluded from our analysis. To test whether our results were affected by the weighting scheme, we also calculated the phenological indicators after changing the moving window, and without using the weighting scheme. The results showed no significant differences compared with the original method (Supplementary Fig. 14b,c). The urban–rural phenological gradients were also evident using these different weighting schemes (Supplementary Fig. 14d,e).

Conversion of urban–rural XCO_2 gradients to surface CO_2 gradients. The XCO_2 data are column-averaged CO_2 mixed ratios, and differ in magnitude from CO_2 concentrations near the surface. Therefore, to investigate the effect of CO_2 fertilization on vegetation phenology, we needed to convert the urban–rural XCO_2 gradients to surface CO_2 gradients. Although atmospheric transport models would be the ideal approach to fulfil this purpose, there are still many precluding issues. First, high-spatial-resolution previous fluxes of CO_2, including anthropogenic emissions and terrestrial carbon uptake, as well as high-resolution meteorological data (wind speed and wind direction), still have large uncertainties, especially in urban areas with highly variable emission sources (such as traffic pollution) and high degrees of surface heterogeneity[90,91]. Second, as one of the main factors that affect the variations of surface CO_2 concentration at finer scales, the heterogeneity of the vertical profile in urban areas induced by buildings can hardly be accurately estimated and illustrated[92]. Third, continuous and highly spatiotemporal ground and satellite CO_2 measurements are still insufficient to provide accurate constraints and evaluations for atmospheric transport models to simulate the high-spatial-resolution surface CO_2 concentrations at large scales[93]. Therefore, global near-surface CO_2 concentrations from atmospheric transport models or flux-inversion systems generally have relatively low spatial resolutions[94], which cannot meet our needs for deriving urban–rural gradients at large scales. Statistical methods are therefore more appropriate for converting XCO_2 gradients to surface CO_2 gradients.

We used two approaches to determine the conversion factors. First, we used a near-surface CO_2 dataset with a comprehensive spatial coverage. The data were obtained in Shanghai during April and May of 2014 and covered the entire urban area, with a total of 172 sample points[95] (Supplementary Fig. 15). The slopes of the near-surface CO_2 measurements and OCO-2 XCO_2 observations in the same city were calculated (Supplementary Fig. 16a,b). The conversion factor could then be obtained ($K = 21.2$). Second, we collected a number of urban–rural surface CO_2 gradients from previous studies (Supplementary Table 2) and then calculated the XCO_2 gradients of these urban clusters and compared them via linear regression (Supplementary Fig. 16c), which indicated that the conversion factor was approximately 28.5. These data from previous studies have an average of seven years' gap with the satellite observations, and thus the observations of urban–rural surface CO_2 gradients may be lower than those of the present, which possibly leads to a higher estimation of the K factor. Therefore, we used a K factor of 25, which is the average value of these two approaches. Then, we converted the urban–rural XCO_2 gradients to surface CO_2 gradients through this conversion factor. This conversion factor was derived via statistical methods that may have some uncertainties. For example, the K factor derived from the first approach was 21.2 ± 8.3, while that from the second approach was 28.5 ± 9.5 (mean $\pm$ s.e.). To test the robustness of our results according to different K values, we repeated our analysis using a wide range of K factors (from 19–30), which was the intersection of ranges of the K factors estimated from these two approaches. The results showed that the partial correlations between urban–rural phenological gradients and CO_2 gradients were not affected by K values, given that this conversion factor was linear (Supplement Fig. 17a). Although the predicted GSL had a declining trend when K was increasing (Supplement Fig. 17b), our predicted GSL shifts (5.9–11.4 d decade^{-1}) based on a K factor of 25 were comparable to the average value of these shifts. These results suggested that the joint control of elevated CO_2 and temperature on urban–rural photosynthetic phenological gradients was robust across different K values.

Analysis. The phenological differences, LST gradients and CO_2 gradients between urban and rural areas for each city were first calculated as:

$$\Delta P = P_{urban} - P_{rural} \qquad (3)$$

where ΔP represents the urban–rural gradients for the phenological indicators (SOS, POS, EOS and GSL), LST and CO_2 concentration, and P_{urban} and P_{rural} represent these values in urban clusters and their corresponding rural buffers, respectively. The LST differences included the mean spring LST (January to May, corresponding to SOS), mean summer LST (June to August, corresponding to POS), mean autumn and winter LST (September to December, corresponding to EOS) and mean annual LST (corresponding to GSL)[38]. Due to the limited OCO-2 observations, we used the whole-year XCO_2 observations and the conversion factor (K) to derive the urban–rural CO_2 gradients. The differences in photosynthetic (SIF) and greenness (EVI) phenology along the urban–rural gradients for different rural buffers (that is, 10, 20, 30 and 40 km) were calculated (Supplementary Fig. 4). Previous studies have shown that the mean footprint of urban areas on phenology is about 20–25 km, which should be able to reflect the background vegetation phenology[21,38,96]. In this analysis, we found that the largest urban–rural phenological differences occurred between urban clusters and 30-km rural buffers. Therefore, we used the 30-km rural buffers as representatives in the subsequent analyses.

The spatial distributions of photosynthetic phenology differences based on latitude, mean annual air temperature and precipitation were then analysed. We also analysed the phenological differences in different climate zones based on the Köppen–Geiger climate zones classification (http://people.eng.unimelb.edu.au/mpeel/koppen.html). To determine the main controlling drivers of urban–rural phenological gradients, we determined the partial correlations of ΔP with latitude, longitude, urban size, mean annual air temperature, annual precipitation, CO_2 gradient (ΔCO_2) and LST gradient (ΔLST). The partial correlation (two tailed) of each factor was determined while controlling for the other factors. To reduce the stochastic error, the LST and CO_2 gradients were binned every $0.15\,°C$ and 1.5 ppm, respectively. Then, we determined the main factors controlling each phenological indicator by analysing the associations of urban–rural phenological gradients with temperature and CO_2 enhancements. Furthermore, we derived their sensitivities with a forward stepwise regression model (Supplementary Table 3). This method automatically repeats the procedures of forward selection and backward elimination. In each step, an explanatory variable is considered to either add or subtract from the set of variables based on a sequence of F tests. Finally, we estimated the near-term projected shifts in photosynthetic phenology by multiplying the sensitivities with LST and CO_2 concentration predictions during 2015–2035 based on four RCP scenarios (RCPs 2.6, 4.5, 6.0 and 8.5).

Finally, we analysed the uncertainty of projected phenophase shifts as a consequence of using LST other than AST to characterize the urban–rural temperature gradients. Vegetation phenology theoretically should respond to AST more than to LST. As shown in previous studies on the impact of land cover on temperature[97], the spatial gradients of AST are probably smaller than those of LST (Supplementary Fig. 18a), which may translate to a higher sensitivity of GSL to AST than to LST (Supplementary Fig. 18b). Therefore, projected shifts of GSL based on urban–rural AST gradients might be larger than those based on LST gradients (Supplementary Fig. 18c; approximately $0.5–0.8\,d\,decade^{-1}$). However, current high-resolution AST datasets are generally based on observations from weather stations, which cannot fully capture the small-scale urban–rural heterogeneity because of the low density of stations. Due to the limitations of the current AST datasets, analyses based on this variable may actually have larger uncertainties than those based on LST, and will need to be investigated further in the future.

Reporting Summary. Further information on research design is available in the Nature Research Reporting Summary linked to this article.

Data availability
OCO-2 SIF and XCO_2 data are available at https://disc.gsfc.nasa.gov/. MODIS EVI and LST data are available at https://ladsweb.modaps.eosdis.nasa.gov/. Precipitation data can be obtained from https://pmm.nasa.gov. Global Historical Climatology Network (version 2) and Climate Anomaly Monitoring System air temperature data are available at https://www.esrl.noaa.gov. Climate Change Initiative land cover data are available at http://maps.elie.ucl.ac.be/CCI/viewer/download.php. GTOPO30 digital elevation model data are available at https://earthexplorer.usgs.gov/. NO_2 and O_3 data are available at http://www.temis.nl/index.php. Projected CO_2 concentrations can be obtained from the RCP Database (http://www.iiasa.ac.at/web-apps/tnt/RcpDb). Model results and the urban clusters are available at https://drive.google.com/drive/folders/1yzcoRAjjubiLDqlg6zbLUCfE_m1mHAsL?usp=sharing.

Code availability
The codes used to estimate the phenological indicators in this study are available at https://drive.google.com/drive/folders/1yzcoRAjjubiLDqlg6zbLUCfE_m1mHAsL?usp=sharing.

References
1. Canadell, J. G. et al. Contributions to accelerating atmospheric CO_2 growth from economic activity, carbon intensity, and efficiency of natural sinks. *Proc. Natl Acad. Sci. USA* **104**, 18866–18870 (2007).
2. Keenan, T. F. et al. Net carbon uptake has increased through warming-induced changes in temperate forest phenology. *Nat. Clim. Change* **4**, 598–604 (2014).
3. Peñuelas, J. & Filella, I. Phenology feedbacks on climate change. *Science* **324**, 887–888 (2009).
4. Richardson, A. D. et al. Climate change, phenology, and phenological control of vegetation feedbacks to the climate system. *Agric. For. Meteorol.* **169**, 156–173 (2013).
5. Richardson, A. D. et al. Ecosystem warming extends vegetation activity but heightens vulnerability to cold temperatures. *Nature* **560**, 368–371 (2018).
6. Peñuelas, J. & Filella, I. Responses to a warming world. *Science* **294**, 793–795 (2001).
7. Piao, S. et al. Net carbon dioxide losses of northern ecosystems in response to autumn warming. *Nature* **451**, 49–52 (2008).
8. Piao, S. et al. Leaf onset in the Northern Hemisphere triggered by daytime temperature. *Nat. Commun.* **6**, 6911 (2015).
9. Fu, Y. H. et al. Declining global warming effects on the phenology of spring leaf unfolding. *Nature* **526**, 104–107 (2015).
10. IPCC *Climate Change 2014: Synthesis Report* (eds Core Writing Team, Pachauri, R. K. & Meyer, L. A.) (IPCC, 2014).
11. Calfapietra, C. et al. Challenges in elevated CO_2 experiments on forests. *Trends Plant Sci.* **15**, 5–10 (2010).
12. Fu, Y. H. et al. Larger temperature response of autumn leaf senescence than spring leaf-out phenology. *Glob. Change Biol.* **24**, 2159–2168 (2017).
13. Wolkovich, E. M. et al. Warming experiments underpredict plant phenological responses to climate change. *Nature* **485**, 494–497 (2012).
14. Calfapietra, C., Peñuelas, J. & Niinemets, Ü. Urban plant physiology: adaptation-mitigation strategies under permanent stress. *Trends Plant Sci.* **20**, 72–75 (2015).
15. Peng, S. et al. Surface urban heat island across 419 global big cities. *Environ. Sci. Technol.* **46**, 696–703 (2011).
16. Schwandner, F. M. et al. Spaceborne detection of localized carbon dioxide sources. *Science* **358**, eaam5782 (2017).
17. Zhao, S., Liu, S. & Zhou, D. Prevalent vegetation growth enhancement in urban environment. *Proc. Natl Acad. Sci. USA* **113**, 6313–6318 (2016).
18. Sun, Y. et al. Overview of solar-induced chlorophyll fluorescence (SIF) from the Orbiting Carbon Observatory-2: retrieval, cross-mission comparison, and global monitoring for GPP. *Remote Sens. Environ.* **209**, 808–823 (2018).
19. Guanter, L. et al. Global and time-resolved monitoring of crop photosynthesis with chlorophyll fluorescence. *Proc. Natl Acad. Sci. USA* **111**, E1327–E1333 (2014).
20. Huete, A. et al. Overview of the radiometric and biophysical performance of the MODIS vegetation indices. *Remote Sens. Environ.* **83**, 195–213 (2002).
21. Zhou, D., Zhao, S., Zhang, L. & Liu, S. Remotely sensed assessment of urbanization effects on vegetation phenology in China's 32 major cities. *Remote Sens. Environ.* **176**, 272–281 (2016).
22. Zhou, D., Zhao, S., Liu, S., Zhang, L. & Zhu, C. Surface urban heat island in China's 32 major cities: spatial patterns and drivers. *Remote Sens. Environ.* **152**, 51–61 (2014).
23. Chuine, I., Morin, X. & Bugmann, H. Warming, photoperiods, and tree phenology. *Science* **329**, 277–278 (2010).
24. Fu, Y. H., Campioli, M., Deckmyn, G. & Janssens, I. A. Sensitivity of leaf unfolding to experimental warming in three temperate tree species. *Agric. For. Meteorol.* **181**, 125–132 (2013).
25. Jeong, S.-J. et al. Application of satellite solar-induced chlorophyll fluorescence to understanding large-scale variations in vegetation phenology and function over northern high latitude forests. *Remote Sens. Environ.* **190**, 178–187 (2017).
26. Kikuzawa, K. Phenological and morphological adaptations to the light environment in two woody and two herbaceous plant species. *Funct. Ecol.* **17**, 29–38 (2003).
27. Daumard, F. et al. A field platform for continuous measurement of canopy fluorescence. *IEEE Trans. Geosci. Remote Sens.* **48**, 3358–3368 (2010).
28. Suni, T. et al. Interannual variability and timing of growing-season CO_2 exchange in a boreal forest. *J. Geophys. Res. Atmos.* **108**, 4265 (2003).
29. Medvigy, D., Jeong, S. J., Clark, K. L., Skowronski, N. S. & Schäfer, K. V. Effects of seasonal variation of photosynthetic capacity on the carbon fluxes of a temperate deciduous forest. *J. Geophys. Res. Biogeosci.* **118**, 1703–1714 (2013).
30. Chen, X., Wang, D., Chen, J., Wang, C. & Shen, M. The mixed pixel effect in land surface phenology: a simulation study. *Remote Sens. Environ.* **211**, 338–344 (2018).

31. Filella, I., Penuelas, J., Llorens, L. & Estiarte, M. Reflectance assessment of seasonal and annual changes in biomass and CO_2 uptake of a Mediterranean shrubland submitted to experimental warming and drought. *Remote Sens. Environ.* **90**, 308–318 (2004).

32. Hilker, T. et al. Remote sensing of photosynthetic light-use efficiency across two forested biomes: spatial scaling. *Remote Sens. Environ.* **114**, 2863–2874 (2010).

33. Walther, S. et al. Satellite chlorophyll fluorescence measurements reveal large-scale decoupling of photosynthesis and greenness dynamics in boreal evergreen forests. *Glob. Change Biol.* **22**, 2979–2996 (2016).

34. Porcar-Castell, A. et al. Linking chlorophyll a fluorescence to photosynthesis for remote sensing applications: mechanisms and challenges. *J. Exp. Bot.* **65**, 4065–4095 (2014).

35. Baker, N. R. Chlorophyll fluorescence: a probe of photosynthesis in vivo. *Annu. Rev. Plant Biol.* **59**, 89–113 (2008).

36. Norton, A. J., Rayner, P. J., Koffi, E. N. & Scholze, M. Assimilating solar-induced chlorophyll fluorescence into the terrestrial biosphere model BETHY-SCOPE v1.0: model description and information content. *Geosci. Model Dev.* **11**, 1517–1536 (2018).

37. White, M. A., Nemani, R. R., Thornton, P. E. & Running, S. W. Satellite evidence of phenological differences between urbanized and rural areas of the eastern United States deciduous broadleaf forest. *Ecosystems* **5**, 260–273 (2002).

38. Zhang, X., Friedl, M. A., Schaaf, C. B., Strahler, A. H. & Schneider, A. The footprint of urban climates on vegetation phenology. *Geophys. Res. Lett.* **31**, L12209 (2004).

39. Han, G. & Xu, J. Land surface phenology and land surface temperature changes along an urban–rural gradient in Yangtze River Delta, China. *Environ. Manag.* **52**, 234–249 (2013).

40. Cong, N. et al. Spring vegetation green-up date in China inferred from SPOT NDVI data: a multiple model analysis. *Agric. For. Meteorol.* **165**, 104–113 (2012).

41. Li, X. et al. Response of vegetation phenology to urbanization in the conterminous United States. *Glob. Change Biol.* **23**, 2818–2830 (2017).

42. Niu, S. et al. Seasonal hysteresis of net ecosystem exchange in response to temperature change: patterns and causes. *Glob. Change Biol.* **17**, 3102–3114 (2011).

43. Van der Tol, C., Verhoef, W. & Rosema, A. A model for chlorophyll fluorescence and photosynthesis at leaf scale. *Agric. For. Meteorol.* **149**, 96–105 (2009).

44. Sun, Y. et al. OCO-2 advances photosynthesis observation from space via solar-induced chlorophyll fluorescence. *Science* **358**, eaam5747 (2017).

45. Zarco-Tejada, P., Morales, A., Testi, L. & Villalobos, F. Spatio-temporal patterns of chlorophyll fluorescence and physiological and structural indices acquired from hyperspectral imagery as compared with carbon fluxes measured with eddy covariance. *Remote Sens. Environ.* **133**, 102–115 (2013).

46. Yang, X. et al. Solar-induced chlorophyll fluorescence that correlates with canopy photosynthesis on diurnal and seasonal scales in a temperate deciduous forest. *Geophys. Res. Lett.* **42**, 2977–2987 (2015).

47. Joiner, J. et al. The seasonal cycle of satellite chlorophyll fluorescence observations and its relationship to vegetation phenology and ecosystem atmosphere carbon exchange. *Remote Sens. Environ.* **152**, 375–391 (2014).

48. CaraDonna, P. J., Iler, A. M. & Inouye, D. W. Shifts in flowering phenology reshape a subalpine plant community. *Proc. Natl Acad. Sci. USA* **111**, 4916–4921 (2014).

49. Menzel, A. et al. European phenological response to climate change matches the warming pattern. *Glob. Change Biol.* **12**, 1969–1976 (2006).

50. Thompson, R. & Clark, R. Is spring starting earlier? *Holocene* **18**, 95–104 (2008).

51. Miller-Rushing, A. J. & Primack, R. B. Global warming and flowering times in Thoreau's Concord: a community perspective. *Ecology* **89**, 332–341 (2008).

52. Vitasse, Y. et al. Leaf phenology sensitivity to temperature in European trees: do within-species populations exhibit similar responses? *Agric. For. Meteorol.* **149**, 735–744 (2009).

53. Piao, S. et al. Weakening temperature control on the interannual variations of spring carbon uptake across northern lands. *Nat. Clim. Change* **7**, 359–363 (2017).

54. Körner, C. & Basler, D. Phenology under global warming. *Science* **327**, 1461–1462 (2010).

55. Way, D. A. & Montgomery, R. A. Photoperiod constraints on tree phenology, performance and migration in a warming world. *Plant Cell Environ.* **38**, 1725–1736 (2015).

56. Gonsamo, A., Chen, J. M. & Ooi, Y. W. Peak season plant activity shift towards spring is reflected by increasing carbon uptake by extratropical ecosystems. *Glob. Change Biol.* **24**, 2117–2128 (2017).

57. Xu, C., Liu, H., Williams, A. P., Yin, Y. & Wu, X. Trends toward an earlier peak of the growing season in Northern Hemisphere mid-latitudes. *Glob. Change Biol.* **22**, 2852–2860 (2016).

58. Wu, C. et al. Contrasting responses of autumn-leaf senescence to daytime and night-time warming. *Nat. Clim. Change* **8**, 1092–1096 (2018).

59. Marchin, R. M., Salk, C. F., Hoffmann, W. A. & Dunn, R. R. Temperature alone does not explain phenological variation of diverse temperate plants under experimental warming. *Glob. Change Biol.* **21**, 3138–3151 (2015).

60. Sigurdsson, B. D. Elevated CO_2 and nutrient status modified leaf phenology and growth rhythm of young *Populus trichocarpa* trees in a 3-year field study. *Trees* **15**, 403–413 (2001).

61. Liu, Q. et al. Delayed autumn phenology in the Northern Hemisphere is related to change in both climate and spring phenology. *Glob. Change Biol.* **22**, 3702–3711 (2016).

62. Cleland, E. E., Chiariello, N. R., Loarie, S. R., Mooney, H. A. & Field, C. B. Diverse responses of phenology to global changes in a grassland ecosystem. *Proc. Natl Acad. Sci. USA* **103**, 13740–13744 (2006).

63. Jach, M. E. & Ceulemans, R. Effects of elevated atmospheric CO_2 on phenology, growth and crown structure of Scots pine (*Pinus sylvestris*) seedlings after two years of exposure in the field. *Tree Physiol.* **19**, 289–300 (1999).

64. Taylor, G. et al. Future atmospheric CO_2 leads to delayed autumnal senescence. *Glob. Change Biol.* **14**, 264–275 (2008).

65. *State of the Climate: Global Climate Report for May 2018* (NOAA National Centers for Environmental Information, 2018); https://www.ncdc.noaa.gov/sotc/global/201805

66. Jeong, S.-J., Ho, C.-H., Gim, H.-J. & Brown, M. E. Phenology shifts at start vs. end of growing season in temperate vegetation over the Northern Hemisphere for the period 1982–2008. *Glob. Change Biol.* **17**, 2385–2399 (2011).

67. Barichivich, J. et al. Large-scale variations in the vegetation growing season and annual cycle of atmospheric CO_2 at high northern latitudes from 1950 to 2011. *Glob. Change Biol.* **19**, 3167–3183 (2013).

68. Buyantuyev, A. & Wu, J. Urbanization diversifies land surface phenology in arid environments: interactions among vegetation, climatic variation, and land use pattern in the Phoenix metropolitan region, USA. *Landsc. Urban Plan.* **105**, 149–159 (2012).

69. Decina, S. M., Templer, P. H. & Hutyra, L. R. Atmospheric inputs of nitrogen, carbon, and phosphorus across an urban area: unaccounted fluxes and canopy influences. *Earths Future* **6**, 134–148 (2018).

70. Gregg, J. W., Jones, C. G. & Dawson, T. E. Urbanization effects on tree growth in the vicinity of New York City. *Nature* **424**, 183–187 (2003).

71. Zhang, X., Friedl, M. A., Schaaf, C. B., Strahler, A. H. & Liu, Z. Monitoring the response of vegetation phenology to precipitation in Africa by coupling MODIS and TRMM instruments. *J. Geophys. Res. Atmos.* **110**, D12103 (2005).

72. Do, F. C. et al. Environmental influence on canopy phenology in the dry tropics. *For. Ecol. Manag.* **215**, 319–328 (2005).

73. Peñuelas, J. et al. Complex spatiotemporal phenological shifts as a response to rainfall changes. *New Phytol.* **161**, 837–846 (2004).

74. Fisher, J. B., Huntzinger, D. N., Schwalm, C. R. & Sitch, S. Modeling the terrestrial biosphere. *Annu. Rev. Environ. Resour.* **39**, 91–123 (2014).

75. Zhou, Y. et al. A cluster-based method to map urban area from DMSP/OLS nightlights. *Remote Sens. Environ.* **147**, 173–185 (2014).

76. Zhou, Y. et al. A global map of urban extent from nightlights. *Environ. Res. Lett.* **10**, 054011 (2015).

77. Huang, X., Schneider, A. & Friedl, M. A. Mapping sub-pixel urban expansion in China using MODIS and DMSP/OLS nighttime lights. *Remote Sens. Environ.* **175**, 92–108 (2016).

78. Zhang, Y. et al. On the relationship between sub-daily instantaneous and daily total gross primary production: implications for interpreting satellite-based SIF retrievals. *Remote Sens. Environ.* **205**, 276–289 (2018).

79. Frankenberg, C. et al. Prospects for chlorophyll fluorescence remote sensing from the Orbiting Carbon Observatory-2. *Remote Sens. Environ.* **147**, 1–12 (2014).

80. Crisp, D. et al. The on-orbit performance of the Orbiting Carbon Observatory-2 (OCO-2) instrument and its radiometrically calibrated products. *Atmos. Meas. Tech.* **10**, 59–81 (2017).

81. Wunch, D. et al. Comparisons of the Orbiting Carbon Observatory-2 (OCO-2) XCO_2 measurements with TCCON. *Atmos. Meas. Tech.* **10**, 2209–2238 (2017).

82. Abatzoglou, J. T., Dobrowski, S. Z., Parks, S. A. & Hegewisch, K. C. TerraClimate, a high-resolution global dataset of monthly climate and climatic water balance from 1958–2015. *Sci. Data* **5**, 170191 (2018).

83. Collier, M. A., et al. The CSIRO-Mk3.6.0 Atmosphere-Ocean GCM: Participation in CMIP5 and data publication in *19th International Congress on Modelling and Simulation, Perth, Australia*, 2691–2697 (2011). http://www.mssanz.org.au/modsim2011/F5/collier.pdf

84. Griffies, S. M. et al. The GFDL CM3 coupled climate model: characteristics of the ocean and sea ice simulations. *J. Clim.* **24**, 3520–3544 (2011).

85. Schmidt, G. A. et al. Configuration and assessment of the GISS ModelE2 contributions to the CMIP5 archive. *J. Adv. Model. Earth Syst.* **6**, 141–184 (2014).

86. Bentsen, M. et al. The Norwegian Earth system model, NorESM1-M—part 1: description and basic evaluation of the physical climate. *Geosci. Model Dev.* **6**, 687–720 (2013).

87. Gonsamo, A., Chen, J. M. & D'Odorico, P. Deriving land surface phenology indicators from CO_2 eddy covariance measurements. *Ecol. Indic.* **29**, 203–207 (2013).

88. Elmore, A. J., Guinn, S. M., Minsley, B. J. & Richardson, A. D. Landscape controls on the timing of spring, autumn, and growing season length in mid-Atlantic forests. *Glob. Change Biol.* **18**, 656–674 (2012).

89. Hird, J. N. & McDermid, G. J. Noise reduction of NDVI time series: an empirical comparison of selected techniques. *Remote Sens. Environ.* **113**, 248–258 (2009).

90. Duren, R. M. & Miller, C. E. Measuring the carbon emissions of megacities. *Nat. Clim. Change* **2**, 560–562 (2012).

91. Bréon, F. et al. An attempt at estimating Paris area CO_2 emissions from atmospheric concentration measurements. *Atmos. Chem. Phys.* **15**, 1707–1724 (2015).

92. Chen, F. et al. The integrated WRF/urban modelling system: development, evaluation, and applications to urban environmental problems. *Int. J. Climatol.* **31**, 273–288 (2011).

93. Chevallier, F. et al. Toward robust and consistent regional CO_2 flux estimates from in situ and spaceborne measurements of atmospheric CO_2. *Geophys. Res. Lett.* **41**, 1065–1070 (2014).

94. Peters, W. et al. An atmospheric perspective on North American carbon dioxide exchange: CarbonTracker. *Proc. Natl Acad. Sci. USA* **104**, 18925–18930 (2007).

95. Liu, M. et al. Spatial variation of near-surface CO_2 concentration during spring in Shanghai. *Atmos. Pollut. Res.* **7**, 31–39 (2016).

96. Zhou, D., Zhao, S., Zhang, L., Sun, G. & Liu, Y. The footprint of urban heat island effect in China. *Sci. Rep.* **5**, 11160 (2015).

97. Alkama, R. & Cescatti, A. Biophysical climate impacts of recent changes in global forest cover. *Science* **351**, 600–604 (2016).

Author contributions

Y. Zhang designed the research. S.W. performed the analysis. S.W., Y. Zhang and W.J. drafted the paper. J.P. and A.C. contributed to interpreting the results and writing the paper. A.H., Y. Zhou and Y.F. contributed to writing the paper. Y. Zhou and M.L. provided the data.

Competing interests

The authors declare no competing interests.

Additional information

Supplementary information is available for this paper at https://doi.org/10.1038/s41559-019-0931-1.

Reprints and permissions information is available at www.nature.com/reprints.

Correspondence and requests for materials should be addressed to Y.Z.

Publisher's note: Springer Nature remains neutral with regard to jurisdictional claims in published maps and institutional affiliations.

Corresponding author(s): Yongguang Zhang

Last updated by author(s): May 21, 2019

Reporting Summary

Nature Research wishes to improve the reproducibility of the work that we publish. This form provides structure for consistency and transparency in reporting. For further information on Nature Research policies, see <u>Authors & Referees</u> and the <u>Editorial Policy Checklist</u>.

Statistics

For all statistical analyses, confirm that the following items are present in the figure legend, table legend, main text, or Methods section.

n/a	Confirmed	
☐	☒	The exact sample size (*n*) for each experimental group/condition, given as a discrete number and unit of measurement
☐	☒	A statement on whether measurements were taken from distinct samples or whether the same sample was measured repeatedly
☐	☒	The statistical test(s) used AND whether they are one- or two-sided *Only common tests should be described solely by name; describe more complex techniques in the Methods section.*
☒	☐	A description of all covariates tested
☒	☐	A description of any assumptions or corrections, such as tests of normality and adjustment for multiple comparisons
☐	☒	A full description of the statistical parameters including central tendency (e.g. means) or other basic estimates (e.g. regression coefficient) AND variation (e.g. standard deviation) or associated estimates of uncertainty (e.g. confidence intervals)
☐	☒	For null hypothesis testing, the test statistic (e.g. F, t, r) with confidence intervals, effect sizes, degrees of freedom and P value noted *Give P values as exact values whenever suitable.*
☒	☐	For Bayesian analysis, information on the choice of priors and Markov chain Monte Carlo settings
☒	☐	For hierarchical and complex designs, identification of the appropriate level for tests and full reporting of outcomes
☐	☒	Estimates of effect sizes (e.g. Cohen's *d*, Pearson's *r*), indicating how they were calculated

Our web collection on <u>statistics for biologists</u> contains articles on many of the points above.

Software and code

Policy information about <u>availability of computer code</u>

Data collection	No software was used for data collection.
Data analysis	We used MATLAB version 2015b.

For manuscripts utilizing custom algorithms or software that are central to the research but not yet described in published literature, software must be made available to editors/reviewers. We strongly encourage code deposition in a community repository (e.g. GitHub). See the Nature Research <u>guidelines for submitting code & software</u> for further information.

Data

Policy information about <u>availability of data</u>

All manuscripts must include a <u>data availability statement</u>. This statement should provide the following information, where applicable:
- Accession codes, unique identifiers, or web links for publicly available datasets
- A list of figures that have associated raw data
- A description of any restrictions on data availability

A data availability statement has been presented in the manuscript. The data of all the analyzes are publicly accessible.

Field-specific reporting

Please select the one below that is the best fit for your research. If you are not sure, read the appropriate sections before making your selection.

☐ Life sciences   ☐ Behavioural & social sciences   ☒ Ecological, evolutionary & environmental sciences

For a reference copy of the document with all sections, see <u>nature.com/documents/nr-reporting-summary-flat.pdf</u>

Ecological, evolutionary & environmental sciences study design

All studies must disclose on these points even when the disclosure is negative.

Study description	This study used 880 urban clusters in the Northern Hemisphere as the natural "urban laboratories", finding that vegetation has unexpected longer photosynthetic seasons in urban areas than previous thought, and, surprisingly, these anomalies are not merely caused by climate warming but also, and more significantly, by the CO_2 enrichment, especially for the autumn phenology.
Research sample	We used 880 urban clusters in the Northern Hemisphere as the research samples.
Sampling strategy	We selected urban clusters with at least eight SIF observations in both the urban cluster and each corresponding buffer to ensure a successful calculation of phenology. This resulted in a total of 880 urban clusters at mid- to high-latitudes in the Northern Hemisphere (NH, ≥30°).
Data collection	The remote sensing datasets and climate data were downloaded from the URLs stated in the article.
Timing and spatial scale	We generally used the remote sensing data from 2015-2017. The OCO-2 SIF and XCO2 data used in this study had a spatial resolution of 1.29 × 2.25 km2. The MODIS EVI data were provided at a 1 km spatial resolution and 16-day temporal resolution over 2015-2017. The MODIS LST data had a spatial resolution of 1 km and a temporal resolution of 8-day. Annual air temperature data had a spatial resolution of 0.5 degree. Monthly GPM precipitation data had a spatial resolution data of 0.1 degree. Global DEM data from GTOPO30 were provided at spatial resolution of 30 arc seconds. Monthly NO2 and O3 data from OMI satellite had a spatial resolution of 0.125 degree and 0.25 degree, respectively.
Data exclusions	No data were excluded from the data sets in all the analyses.
Reproducibility	Our results were mainly based on the public satellite data, thus the results could be reproduced.
Randomization	We performed the analysis for all of the 880 urban clusters, so randomization is not relevant to this study.
Blinding	Most of our study were based on the existing satellite data, so blinding is not relevant to this study.

Did the study involve field work? ☐ Yes ☒ No

Reporting for specific materials, systems and methods

We require information from authors about some types of materials, experimental systems and methods used in many studies. Here, indicate whether each material, system or method listed is relevant to your study. If you are not sure if a list item applies to your research, read the appropriate section before selecting a response.

Materials & experimental systems

n/a	Involved in the study
☒	☐ Antibodies
☒	☐ Eukaryotic cell lines
☒	☐ Palaeontology
☒	☐ Animals and other organisms
☒	☐ Human research participants
☒	☐ Clinical data

Methods

n/a	Involved in the study
☒	☐ ChIP-seq
☒	☐ Flow cytometry
☒	☐ MRI-based neuroimaging